JOURNAL OF COMPUTATIONAL PHYSICS 88, 86–113 (1990)

Viscous Effects on Propagation and Reflection of Solitary Waves in Shallow Channels

C. J. TANG, V. C. PATEL, AND L. LANDWEBER

Department of Mechanical Engineering and Iowa Institute of Hydraulic Research, University of Iowa, Iowa City, Iowa 52242-1585

Received July 29, 1988; revised May 30, 1989

A numerical method for the solution of the Navier–Stokes equations for flows with a free surface, with emphasis on the exact kinematic and dynamic boundary conditions at the free surface, is described. The method is used to study the propagation of a solitary wave in a shallow channel, and the reflection of such a wave from a vertical wall. The numerical results are compared with analytical solutions which neglect or simplify the effects of viscosity and surface tension. © 1990 Academic Press, Inc.

1. INTRODUCTION

The investigation of a nonlinear long wave, such as a tsunami, traveling in shallow water near the shore, is important in the design of coastline and harbor structures. In classical two-dimensional, long-wave theory, the inviscid approximation is usually made in a perturbation analysis to obtain either the Korteweg–de Vries equation in the case of unidirectional propagation or the Boussinesq equation for waves moving in two directions. Based on this theory, the interesting result was obtained that the tendency of nonlinear effects to increase the wave slope is balanced by the dispersion of the wave system, and, therefore, the wave profile is preserved during the propagation. However, if viscosity of the fluid is considered, energy dissipation will reduce the wave amplitude. To analyze these complexities, including nonlinear effects, dispersion, and dissipation, a more general formulation is required. Solutions of the Navier–Stokes equations with consistent viscous boundary conditions offer an opportunity to capture these phenomena. Because closed-form analytic solutions probably do not exist, we present here numerical solutions of the two-dimensional Navier-Stokes equations with the complete set of viscous boundary conditions applied at the free surface.

Recent work in computational fluid dynamics has led to many numerical methods for the solution of the Navier–Stokes equations. However, many of these are restricted to steady two-dimensional flows, and most to flows without free surfaces. On the other hand, numerical methods which account for free surfaces are based on the assumption of an inviscid fluid. The very few methods which include both free surfaces and viscosity appear to use the marker-and-cell (MAC) technique

0021-9991/90 $3.00

which was introduced by Harlow and Welch [1]. They used markers, in the Lagrangian sense, to trace the motion of fluid particles at the free surface and within the flow region. The SUMMAC (Stanford University modified MAC) method [2] refined some cumbersome parts of the MAC method and used, instead, Eulerian markers at the free surface to indicate the geometry of the free surface.

In the present study, an efficient and stable numerical method is proposed for solving unsteady, two-dimensional, free-surface flow problems. Certain features of the MAC and SUMMAC methods are combined with the SIMPLER (semi-implicit method for pressure-linked equations revised) algorithm of Patankar [3], which has been used with considerable success in the coupling of the momentum and continuity equations, and the finite-analytic (FA) method of Chen and Chen [4], which employs analytical solutions of the linearized equations to discretize the nonlinear momentum equations. This general method is used to study the viscous damping of a solitary wave in a channel of constant depth, and the reflection of such a wave from a vertical wall. In both cases, comparisons are made with the available solutions to explicate the effect of viscosity.

2. Governing Equations and Boundary Conditions

The Navier–Stokes equations for two-dimensional, unsteady flow, nondimensionalized with the depth h and velocity $\sqrt{gh}$, where g is the gravitational constant, are

$$\mathrm{Re}\left[\frac{\partial u}{\partial t}+u\frac{\partial u}{\partial x}+v\frac{\partial u}{\partial y}+\frac{\partial p}{\partial x}\right]=\frac{\partial^2 u}{\partial x^2}+\frac{\partial^2 u}{\partial y^2} \tag{1}$$

$$\mathrm{Re}\left[\frac{\partial v}{\partial t}+u\frac{\partial v}{\partial x}+v\frac{\partial v}{\partial y}+\frac{\partial p}{\partial y}\right]=\frac{\partial^2 v}{\partial x^2}+\frac{\partial^2 v}{\partial y^2} \tag{2}$$

and the equation of continuity is

$$\frac{\partial u}{\partial x}+\frac{\partial v}{\partial y}=0, \tag{3}$$

where $\mathrm{Re}=\rho\sqrt{gh}\,h/\mu$ is the Reynolds number, (u, v) are the horizontal and vertical velocity components in the (x, y) directions, respectively (see Fig. 1), t is time, p is the piezometric pressure (i.e., $p=p^*+y$, p^* being the static pressure), ρ is the fluid density, and μ is the viscosity coefficient.

For the solution of Eqs. (1) to (3), it is necessary to define a solution domain and to provide appropriate boundary conditions at all boundaries of that domain, and the initial conditions at $t=0$ in the whole domain. For a typical wave-propagation problem, we choose the computational domain shown in Fig. 1. The conditions at

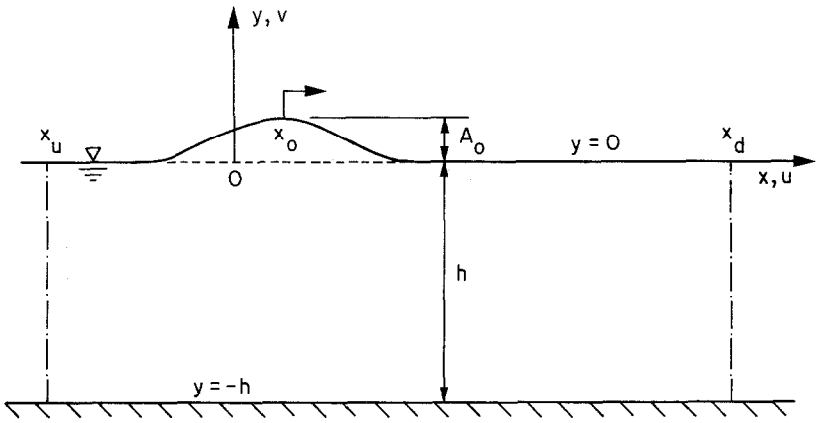

FIG. 1. Wave in a channel; notation and coordinates.

the upstream boundary, $x = x_u$, and those on the channel bottom ($y = -h$) are the same, i.e.,

$$u = v = 0. \tag{4}$$

If it is necessary to specify conditions at the downstream boundary $x = x_d$, the most appropriate is

$$\frac{\partial u}{\partial x} = 0. \tag{5}$$

However, if there is a vertical wall at the boundary, the conditions at the junction of the wall and the free surface are not known. Herein, we shall ignore the nonslip condition along this wall, i.e., ignore the thin boundary layer along it, and apply

$$\frac{\partial v}{\partial x} = 0, \qquad u = 0 \tag{6}$$

at two numerical grid points just beneath the free surface in unsteady-flow calculations to determine the moving contact point.

More complicated boundary conditions apply at the free surface because of its unknown location, and the effects of viscosity and surface tension. The kinematic condition that fluid particles at the free surface remain on the free surface is $DF/Dt = 0$, where $F(x, y, t) = 0$ is the equation of the free surface. If the surface profile is defined by

$$F = y - \eta(x, t) \tag{7}$$

then the kinematic condition becomes

$$\frac{\partial \eta}{\partial t} + u \frac{\partial \eta}{\partial x} = v. \tag{8}$$

For dynamic boundary conditions at a liquid–gas interface, with negligible viscous stresses in the gas, we have, in general,

$$n_i \sigma_{ij} n_j = \frac{k}{\mathrm{We}}; \qquad \tau_i \sigma_{ij} n_j = 0, \tag{9}$$

where σ_{ij} is the stress tensor

$$\sigma_{ij} = -(p - y)\, \delta_{ij} + \frac{1}{\mathrm{Re}} \left(\frac{\partial u_i}{\partial x_j} + \frac{\partial u_j}{\partial x_i} \right) \tag{10}$$

in the liquid, n_i and τ_i are unit vectors, normal and tangential to the free surface, respectively, δ_{ij} is the Kronecker delta, k is the curvature of the free surface, and We is the Weber number, defined by $\mathrm{We} = \rho g h^2/\sigma$, σ being the coefficient of surface tension. For the present two-dimensional problem, with the free surface given by Eq. (7), we have

$$k = \frac{\partial^2 \eta / \partial x^2}{[1 + (\partial \eta / \partial x)^2]^{3/2}}$$

and Eqs. (9) reduce to

$$p_0 = \eta + \frac{2[(\partial \eta/\partial x)^2\, \partial u/\partial x - (\partial u/\partial y + \partial v/\partial x)\, \partial \eta/\partial x + \partial v/\partial y]}{\mathrm{Re}[1 + (\partial \eta/\partial x)^2]} - \frac{k}{\mathrm{We}}, \tag{11}$$

where

$$p_0(x) = p(x, \eta)$$

and

$$2\left(\frac{\partial u}{\partial x} - \frac{\partial v}{\partial y} \right) \frac{\partial \eta}{\partial x} + \left(\frac{\partial u}{\partial y} + \frac{\partial v}{\partial x} \right) \left[\left(\frac{\partial \eta}{\partial x} \right)^2 - 1 \right] = 0, \tag{12}$$

respectively. Substituting Eqs. (3) and (12) into Eq. (11) yields

$$p_0 = \eta + \frac{2[1 + (\partial \eta/\partial x)^2]}{\mathrm{Re}[1 - (\partial \eta/\partial x)^2]} \frac{\partial v}{\partial y} - \frac{k}{\mathrm{We}}. \tag{13}$$

In summary, the boundary conditions at the free surface of a viscous liquid are expressed by Eqs. (8), (12), and (13). Because of the complexity and difficulty of

handling these conditions, most previous investigators have introduced simplifications and approximations in the treatment of viscous effects at the free surface. In the present study, we apply the complete boundary conditions in the numerical solutions.

The initial free-surface profile of a solitary wave is taken to be that given by the closed-form formulation of Boussinesq, i.e.,

$$\eta = A_0 \operatorname{sech}^2[\tfrac{1}{2}(x - x_0)\sqrt{3A_0}] \tag{14}$$

in which A_0 is the maximum height of the wave and x_0 is the location of the wave crest. The initial velocity field was obtained numerically from a stream function which satisfies the Laplace equation with the conditions of constant values at the bottom and the free surface, and linear variation between these two constants at the upstream and the downstream ends of the solution domain. An initial condition for the pressure field is not necessary because the pressure is implicitly determined by the specified velocity field.

3. Numerical Method

3.1. *Linearization and Solution of Momentum Equations*

The Navier–Stokes equations (1) and (2) are first linearized and written in the form

$$\frac{\partial^2 u}{\partial x^2} + \frac{\partial^2 u}{\partial y^2} = \mathrm{Re}\left(\frac{\partial u}{\partial t} + U\frac{\partial u}{\partial x} + V\frac{\partial u}{\partial y} + \frac{\partial p}{\partial x} + S_u\right) \tag{15}$$

$$\frac{\partial^2 v}{\partial x^2} + \frac{\partial^2 v}{\partial y^2} = \mathrm{Re}\left(\frac{\partial v}{\partial t} + U\frac{\partial v}{\partial x} + V\frac{\partial v}{\partial y} + \frac{\partial p}{\partial y} + S_v\right), \tag{16}$$

where U, V are mean values of u, v within a numerical element, and S_u and S_v represent source terms correcting for the linearization. These linear equations can be solved by a variety of methods. For numerical solutions, the value of a variable at a particular node is expressed in terms of those at the neighboring nodes, with coefficients obtained by various formulations, for example, Taylor-series expansions in finite-difference methods. In the FA method of Chen and Chen [4] used here, analytic expressions for these coefficients are obtained in the form of Fourier series, and the variable at the central node is expressed in terms of the eight surrounding nodes of a rectangular element in the two-dimensional case. Tests have shown that the FA method gives a very stable and accurate solution for flows at various Reynolds numbers. A minor disadvantage of the method is that it requires considerable effort to calculate the coefficients, each of which is expressed as the sum of a series. This is alleviated in the present study without loss of numerical stability by using simplified analytic expressions for the coefficients.

Equations (15) and (16) are written in the form

$$\frac{\partial^2\psi}{\partial x^2}+\frac{\partial^2\psi}{\partial y^2}-A\frac{\partial\psi}{\partial x}-B\frac{\partial\psi}{\partial y}-C\frac{\partial\psi}{\partial t}=G_\psi, \tag{17}$$

where ψ stands for either u or v, and the constant coefficients are

$$A=\mathrm{Re}\,U, \qquad B=\mathrm{Re}\,V, \qquad C=\mathrm{Re}$$

$$G_u=\mathrm{Re}\frac{\partial p}{\partial x}+S_u$$

$$G_v=\mathrm{Re}\frac{\partial p}{\partial y}+S_v$$

$$S_\psi=\mathrm{Re}\left[(u-U)\frac{\partial\psi}{\partial x}+(v-V)\frac{\partial\psi}{\partial y}\right].$$

In a small numerical cell, as shown in Fig. 2a, we split Eq. (17) into two,

$$\frac{\partial^2\psi}{\partial x^2}-A\frac{\partial\psi}{\partial x}=F_1 \tag{18}$$

$$\frac{\partial^2\psi}{\partial y^2}-B\frac{\partial\psi}{\partial y}=F_2, \tag{19}$$

in which the unknown nonhomogeneous terms F_1 and F_2 are constants over a cell and must satisfy the condition

$$F_1+F_2-C\frac{\partial\psi}{\partial t}=G_\psi. \tag{20}$$

A general solution of Eq. (18) is a linear combination of exponential and linear functions of x, i.e.,

$$\psi=ae^{Ax}+b-\frac{F_1}{A}x,$$

in which the coefficients a and b can be eliminated by using the boundary conditions $\psi(h_e,0)=\psi_e$, $\psi(-h_w,0)=\psi_w$, and $\psi(0,0)=\psi_p$, i.e.,

$$F_1=-\frac{A}{H'}\left[H_e(\psi_p-\psi_w)-H_w(\psi_e-\psi_p)\right], \tag{21}$$

where

$$H_e=\exp(A\,h_e)-1$$

$$H_w=1-\exp(-A\,h_w)$$

$$H'=h_wH_e-h_eH_w.$$

Likewise, the nonhomogeneous term in Eq. (19) is

$$F_2 = -\frac{B}{H''}\left[H_n(\psi_p - \psi_s) - H_s(\psi_n - \psi_p)\right], \tag{22}$$

where

$$H_n = \exp(B\,h_n) - 1$$
$$H_s = 1 - \exp(-B\,h_s)$$
$$H'' = h_s H_n - h_n H_s$$

in which $\psi(0, h_n) = \psi_n$ and $\psi(0, -h_s) = \psi_s$. If we approximate $\partial\psi/\partial t$ by a backward difference, i.e.,

$$\frac{\partial\psi}{\partial t} = \frac{\psi_p^n - \psi_p^{n-1}}{\Delta t},$$

where ψ_p^n and ψ_p^{n-1} are, respectively, the values at the current and previous time steps, then, from Eqs. (20), (21), and (22), we obtain the discretization formula

$$\psi_p^n = C_e\,\psi_e^n + C_w\psi_w^n + C_n\psi_n^n + C_s\psi_s^n + C_b\psi_p^{n-1} - C_p G_\psi^n \tag{23}$$

in which the FA coefficients are

$$C_e = \frac{AH_w}{HH'}, \qquad C_w = \frac{AH_e}{HH'}, \qquad C_n = \frac{BH_s}{HH''}, \qquad C_s = \frac{BH_n}{HH''},$$

$$C_b = \frac{C}{\Delta t\,H}, \qquad C_p = \frac{1}{H},$$

$$H = \frac{A}{H'}(H_e + H_w) + \frac{B}{H''}(H_n + H_s) + \frac{C}{\Delta t}.$$

In short, Eq. (23) is expressed in the form

$$\psi_p^n = \sum C_{\mathrm{NB}}\,\psi_{\mathrm{NB}}^n|_p + C_b\,\psi_p^{n-1} - C_p\,G_\psi^n, \tag{24}$$

where the subscript NB represents the "neighboring" nodes of P. We note that the various coefficients in this equation contain the mean values U and V resulting from the linearization of the original Navier–Stokes equations. Referring to Fig. 2b, these are evaluated at particular nodes by simple interpolations, e.g.,

$$U_e = u_e$$
$$V_e = [(v_{ne} + v_{se})\,\Delta x_P + (v_n + v_s)\,\Delta x_E]/[2(\Delta x_P + \Delta x_E)]$$

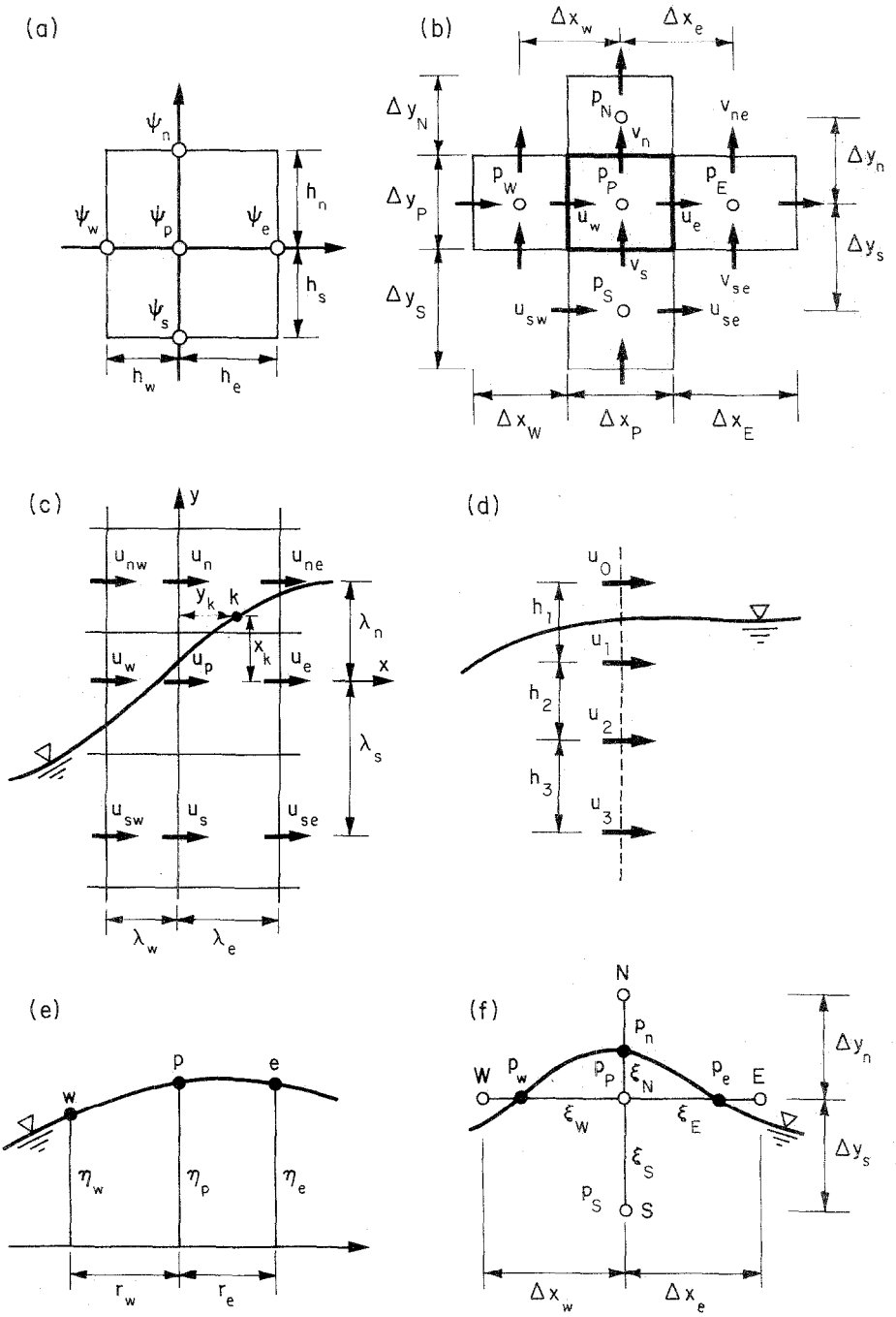

FIG. 2. Symbols in the numerical scheme.

and

$$U_s = [(u_{sw} + u_{se})\,\Delta y_P + (u_e + u_w)\,\Delta y_S]/[2(\Delta y_P + \Delta y_S)]$$
$$V_s = v_s.$$

The coefficients C_e, C_w, C_n, C_s, and C_b are all positive and less than 1, with the sum equal to 1, which yields a stable scheme. Since the corner nodes in the neighborhood of P are not included in this simplified five-point version of the FA method, it is not as accurate as the complete nine-point FA method [4] which includes the corner points. If the numerical grid is carefully chosen to avoid very large mesh aspect ratios, however, the error due to this simplification is not severe.

The linearized Navier–Stokes equations are coupled through the unknowns u, v, and p, and therefore, in principle, they require a simultaneous solution. In the present scheme, we use the x-component momentum equation to solve for u and consider other variables, such as v and $\partial p/\partial x$, as given values from the previous time or iteration. Similarly, the y-component momentum equation is solved for v. The variable p is implicitly determined by letting the velocity field satisfy the continuity equation. The algorithm is outlined in the next section.

3.2. *Solution of Continuity Equation*

The SIMPLER algorithm [3] is used to couple the velocity and pressure fields. A staggered numerical grid, with the velocity and pressure nodes located as shown in Fig. 2b, is used. The nodes of u and v are located at the boundaries of a control volume while that or pressure is centered. Capital letters (E, W, P, N, S) will be used to denote the pressure nodes and lowercase letters (e, w, n, s) for the velocity nodes. Also, the distances between velocity nodes will be denoted by Δx_E, Δy_N, etc., and those between the pressure nodes by Δx_e, Δy_n, etc.

Using central-difference expansions, the continuity equation (3) is written in the form

$$D = \frac{1}{\Delta x_P}(u_e - u_w) + \frac{1}{\Delta y_P}(v_n - v_s) = 0. \tag{25}$$

By applying Eq. (23) at point e for velocity u, we have

$$u_e = \hat{u}_e - d_e(p_E - p_P), \tag{26}$$

where $\hat{u}_e$ is the pseudovelocity defined by

$$\hat{u}_e = \left(\sum C_{\mathrm{NB}}\, u_{\mathrm{NB}}\right)\Big|_e - (C_p S_u)|_e \tag{27}$$

the coefficient of the pressure-difference term is defined in Eq. (29), quantities with the notation $|_e$ are evaluated at the node of u_e, and the subscript NB stands for the neighboring nodes of u_e (see Eqs. (23) and (24)). If the velocities at the west, north,

and south sides are expressed in a similar manner and substituted in Eq. (25), we obtain the following equation for pressure:

$$p_P = a_e p_E + a_w p_W + a_n p_N + a_s p_S - a_P \hat{D} \tag{28}$$

$$a_P = \frac{1}{\Delta x_P}(d_e + d_w) + \frac{1}{\Delta y_P}(d_n + d_s)$$

$$a_e = \frac{d_e}{a_P \Delta x_P}, \qquad a_w = \frac{d_w}{a_P \Delta x_P}, \qquad a_n = \frac{d_n}{a_P \Delta y_P}, \qquad a_s = \frac{d_s}{a_P \Delta y_P}$$

$$d_e = \frac{\mathrm{Re}\, C_{p|e}}{\Delta x_e}, \qquad d_w = \frac{\mathrm{Re}\, C_{p|w}}{\Delta x_w}, \qquad d_n = \frac{\mathrm{Re}\, C_{p|n}}{\Delta x_n}, \qquad d_s = \frac{\mathrm{Re}\, C_{p|s}}{\Delta x_s}$$

$$\hat{D} = \frac{1}{\Delta x_P}(\hat{u}_e - \hat{u}_w) + \frac{1}{\Delta y_P}(\hat{v}_n - \hat{v}_s). \tag{29}$$

If the velocity field is calculated from the discretized momentum equations (26) etc., the pressure can be obtained from Eq. (28). A new set of velocities u, v can be updated from the discretized momentum equations by using this pressure. In practice, several such iterations are necessary to obtain a convergent solution. It is found that these iterations converge rather slowly because the continuity equation is not explicitly satisfied in every iteration cycle. In order to accelerate the convergence, the pressure, obtained from Eq. (28), must be corrected so that the associated velocity field satisfies the continuity equation.

If we denote the approximate velocities and pressure by (u^*, v^*) and p^*, respectively, the velocities calculated from Eq. (26) with p^* are

$$u_e^* = \hat{u}_e^* - d_e(p_E^* - p_P^*), \qquad \text{etc.}$$

If these are subtracted from the exact expressions, i.e., Eq. (24) with the correct p, we have

$$u_e = u_e^* = \hat{u}_e - \hat{u}_e^* - d_e(p'_E - p'_P), \qquad \text{etc.},$$

where the pressure deviation p' $(=p-p^*)$ and the terms $(u-u^*)$, $(\hat{u}-\hat{u}^*)$, etc., are corrections corresponding to the velocity and pseudovelocity fields, respectively. Because all of these corrections vanish when the solution has converged, approximations in these relations only affect the intermediate solution but not the final one. Thus, the correction of the pseudovelocity field, $(\hat{u}-\hat{u}^*)$, etc., may be neglected without any error in the final solution. This critical approximation was applied by Patankar [3] in his SIMPLER algorithm. In the present study, the same approach is used so that the velocities are approximately related to the pressure corrections in the form

$$u_e = u_e^* - d_e(p'_E - p'_P), \qquad \text{etc.} \tag{30}$$

Substitution into the continuity equation (25) then yields the pressure-correction equation

$$p'_P = a_e p'_E + a_w p'_W + a_n p'_N + a_s p'_S - a_P D^*, \tag{31}$$

where

$$D^* = \frac{1}{\Delta x_P}(u_e^* - u_w^*) + \frac{1}{\Delta y_P}(v_n^* - v_s^*) \tag{32}$$

and the other coefficients are exactly the same as in Eq. (29). After the pressure correction is determined from Eq. (31), we use this in Eq. (30) to update the velocity field, keeping the pressure field fixed. The pressure field is then updated by this new velocity field. The solution procedure is outlined in a later section.

3.3. *Treatment of the Free Surface*

The treatment of the free-surface boundary conditions described in Section 2 is the most important part of the present problem. There are three elements in the procedure used to take the free surface into account: determination of the free-surface geometry; updating the conditions at the free surface; and linking the free surface with the fluid interior. Basically, marked particles of the MAC or SUMMAC method are employed to determine the instantaneous location of the free surface in either the Lagrangian sense (MAC method) or the Eulerian sense (SUMMAC method). This is conceptually equivalent to satisfying the kinematic condition at the free surface. In addition, two dynamic boundary conditions have to be satisfied at the free surface. Due to the nonlinearity and coupling of unknowns in these conditions, several global iterations, including the entire flow domain and the free surface, are required to obtain a converged solution at an instant of time.

(a) *Determination of Free-Surface Geometry*

The kinematic condition at the free surface, Eq. (8), is applied to determine the locations of marked particles at the free surface, i.e., the geometry of the free surface. Before solving Eq. (8), it is necessary to interpolate the velocity field at the location of every marked particle (at the free surface) from the main body of the fluid. For this purpose, a second-order interpolation formula is obtained from a Taylor-series expansion. If, for instance, a point at the free surface is located at (x_k, y_k) in the local numerical-grid system, as shown in Fig. 2(c), then the x-component of velocity at this point is represented by

$$u_k = u_p + x_k\left(\frac{\partial u}{\partial x}\right)_p + y_k\left(\frac{\partial u}{\partial y}\right)_p + \frac{1}{2}x_k^2\left(\frac{\partial^2 u}{\partial x^2}\right)_p + \frac{1}{2}y_k^2\left(\frac{\partial^2 u}{\partial y^2}\right)_p + x_k y_k\left(\frac{\partial^2 u}{\partial x\,\partial y}\right)_p, \tag{33}$$

where

$$\left(\frac{\partial^2 u}{\partial x^2}\right)_p = \frac{2}{R_{ew}}\left[\lambda_e u_w + \lambda_w u_e - (\lambda_e + \lambda_w)\, u_p\right]$$

$$\left(\frac{\partial u}{\partial x}\right)_p = \frac{1}{R_{ew}}\left[\lambda_w^2 u_e - \lambda_e^2 u_w + (\lambda_e^2 - \lambda_w^2)\, u_p\right]$$

$$\left(\frac{\partial^2 u}{\partial y^2}\right)_p = \frac{2}{R_{ns}}\left[\lambda_n u_s + \lambda_s u_n - (\lambda_n + \lambda_s)\, u_p\right]$$

$$\left(\frac{\partial u}{\partial y}\right)_p = \frac{1}{R_{ns}}\left[\lambda_s^2\, u_n - \lambda_n^2\, u_s + (\lambda_n^2 - \lambda_s^2)\, u_p\right]$$

$$\left(\frac{\partial^2 u}{\partial x\, \partial y}\right)_p = \frac{1}{R_{ns}}\left[\lambda_s^2 \left(\frac{\partial u}{\partial x}\right)_n - \lambda_n^2 \left(\frac{\partial u}{\partial x}\right)_s + (\lambda_n^2 - \lambda_s^2)\left(\frac{\partial u}{\partial x}\right)_p\right]$$

$$R_{ew} = \lambda_e \lambda_w (\lambda_e + \lambda_w)$$

$$R_{ns} = \lambda_n\, \lambda_s (\lambda_n + \lambda_s)$$

and expressions of $(\partial u/\partial x)_n$ and $(\partial u/\partial x)_s$, similar to $(\partial u/\partial x)_p$, are evaluated at $y = \lambda_n$ and $y = -\lambda_s$, respectively. The expression for v_k is similar to that of u_k.

The (fictitious) values of u above the free surface are obtained by a three-point extrapolation,

$$u_0 = a_1 u_1 - a_2 u_2 + a_3 u_3, \tag{34}$$

where

$$a_1 = \frac{(h_1 + h_2)(h_1 + h_2 + h_3)}{h_1 (h_2 + h_3)}, \qquad a_2 = \frac{h_1}{h_2 h_3}(h_1 + h_2 + h_3), \qquad a_3 = \frac{h_1 (h_1 + h_2)}{h_3 (h_2 + h_3)}$$

and h_1, h_2, h_3 are defined in Fig. 2d. The extrapolation formula for v_0 is similar. These expressions, combined with Eq. (33), give the desired velocities at the free surface.

Once the velocity of each marked particle is known, the location of the free surface can be determined by moving these particles to their new locations in time period Δt. There are two methods to do this. One uses the Lagrangian marker to satisfy the explicit expressions

$$\begin{aligned} x_k &= x_k^{n-1} + u_k \Delta t \\ y_k &= y_k^{n-1} + v_k \Delta t, \end{aligned} \tag{35}$$

where the superscript $n-1$ stands for the values evaluated at the previous time step. The other employs Eulerian markers, implicitly satisfying the kinematic condition of Eq. (8). Using central differences in space and an implicit scheme in time, this may be represented by the finite-difference formula

$$b_e \eta_e + b_p \eta_p + b_w \eta_w = b_s, \tag{36}$$

where the coefficients are

$$b_e = \frac{1}{G_{ew}} u_p \Delta t\, r_w^2, \qquad b_w = -\frac{1}{G_{ew}} u_p \Delta t\, r_e^2$$

$$b_p = 1 - b_e - b_w, \qquad b_s = v_k \Delta t + \eta_p^{n-1}$$

$$G_{ew} = r_e e_w (r_e + r_w),$$

and r_e, r_w are distances projected on the x-axis from a particular particle to two neighboring particles at the free surface, as shown in Fig. 2e. It should be mentioned that in order to maintain stability the time step Δt used in both methods is restricted to a specific small value which ensures that multiple values of η do not result for any marker as it moves on the free surface. Also, it was found from numerical experiments that the results of the two methods do not differ significantly if the iterative solutions at each time step converge. Although both methods were investigated, the second, more implicit method was preferred because it offers the possibility of iterative updates during the time step.

(b) *Updating the Free-Surface Conditions*

Generally speaking, for a two-dimensional viscous flow with a free surface, there are four unknowns, u, v, p, and η, to be determined using the dynamic and kinematic conditions at the free surface. Except for the kinematic condition, which is applied to determine the elevation of the free surface η, only two dynamic conditions remain. Because u, v, and p are coupled together in the governing equations, these two conditions are enough to determine a unique solution. In the present study, the normal component of the dynamic condition, Eq. (13), is used to specify the pressure at the free surface, while the tangential component, Eq. (12), is applied to update the velocity u there. Other variables in the dynamic conditions are chosen as values calculated in the previous iteration.

To introduce exactly the specified pressure condition at the free surface, the pressure near the free surface must be interpolated by means of an "irregular star" formulation which satisfies the discretized Poisson equation [2]:

$$p_P = d_E p_E + d_W p_W + d_N p_N + d_S p_S - \tfrac{1}{2} d_P S_p, \tag{37}$$

where

$$d_E = \frac{d_P}{\xi_E(\xi_E + \xi_W)}, \qquad d_W = \frac{d_P}{\xi_W(\xi_E + \xi_W)},$$

$$d_N = \frac{d_P}{\xi_N(\xi_N + \xi_S)}, \qquad d_S = \frac{d_P}{\xi_S(\xi_N + \xi_S)},$$

$$d_P = \frac{\xi_E \xi_W \xi_N \xi_S}{\xi_E \xi_W + \xi_N \xi_S},$$

and $\xi_E, \xi_W, \xi_N, \xi_S$ are the starred distances as shown in Fig. 2f. Here the source term $S_p = D/\Delta t$ has been modified from the SUMMAC method to fit the present implicit scheme. Using this pressure expression, we are able to impose the exact pressure condition (13) at the free surface.

Second, for the tangential component of the dynamic condition, Eq. (12) is rewritten in the form

$$\frac{\partial u}{\partial y} = \frac{\partial v}{\partial x} + \frac{4}{(\partial \eta/\partial x)^2 - 1} \frac{\partial v}{\partial y} \frac{\partial \eta}{\partial x} = S_q,$$

whence we obtain, in the same second-order finite-difference form,

$$u_0 = a_1 u_1 + a_2 u_2 + a_3 u_3 + S_q, \tag{38}$$

where

$$a_1 = -\frac{2h_1 + 2h_2 + h_3}{h_2(h_2 + h_3)}, \qquad a_2 = \frac{2h_1 + h_2 + h_3}{h_2 h_3} \qquad a_3 = -\frac{2h_1 + h_2}{h_3(h_2 + h_3)}.$$

The lengths h_1, h_2, h_3 and velocities u_0, u_2, u_3 are defined in Fig. 2d. Equation (38) is used to update the x-component of the velocity at the free surface. With regard to v at the free surface, the value is determined so that the continuity equation is satisfied, or is evaluated by extrapolation from inside the fluid, analogous to Eq. (38).

3.4. *Solution Procedure*

To summarize, the complete solution procedure is as follows:

1. Specify the initial conditions for the veloity field and the free-surface profile.
2. For each time step:
   a. Calculate the FA coefficients in the discretized momentum equations (23) and the pseudovelocity field from Eqs. (27), etc.
   c. Calculate pressure near the free surface by the irregular star formulation (37) as boundary conditions of p.
   d. Solve Eq. (28) for pressure with boundary conditions obtained from c. Several iterations are necessary for a converged result.
   e. Solve for u^*, v^* from Eqs. (26), etc. (i.e., u, v in these equations) with conditions (4) and (5) or (6). Several iterations are required for a converged solution.
   f. Determine the mass source D^* from Eq. (32).
   g. Solve for corrections of pressure p' from Eqs. (31). Several iterations are required for a converged solution.

h. Correct the approximate velocity components u^*, v^*, from Eqs. (30), etc., but do not correct the pressure.

i. Update the tangential component of the dynamic conditions to obtain u, v at the free surface from Eq. (38).

j. Interpolate to find the velocity of marked particles from Eq. (33). Update the free surface by either Lagrangian or Eulerian markers from Eqs. (35) or (36).

k. Update conditions at boundaries other than the free surface.

l. Repeat steps a through k until the velocity and pressure fields converge within a prescribed level.

3. Proceed to the next time step.

4. Viscous Damping of a Solitary Wave

The first test problem is the viscous damping of a solitary wave in a long, two-dimensional, shallow water channel. Solitary waves in water were studied experimentally by Russell in 1837. A century later, an analytical solution was first found by Keulegan [5]. Keulegan's solution was rederived by Mei [6] using a perturbation method. The viscous damping considered in this solution was only that due to the boundary layer at the bottom of the channel. The approximate result is

$$A^{-1/4} = A_0^{-1/4} + \frac{0.08356t}{\sqrt{\mathrm{Re}}}, \tag{39}$$

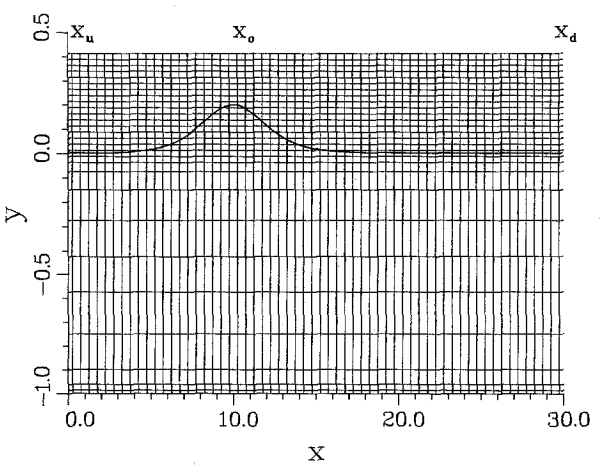

Fig. 3. Solution domain and numerical grid.

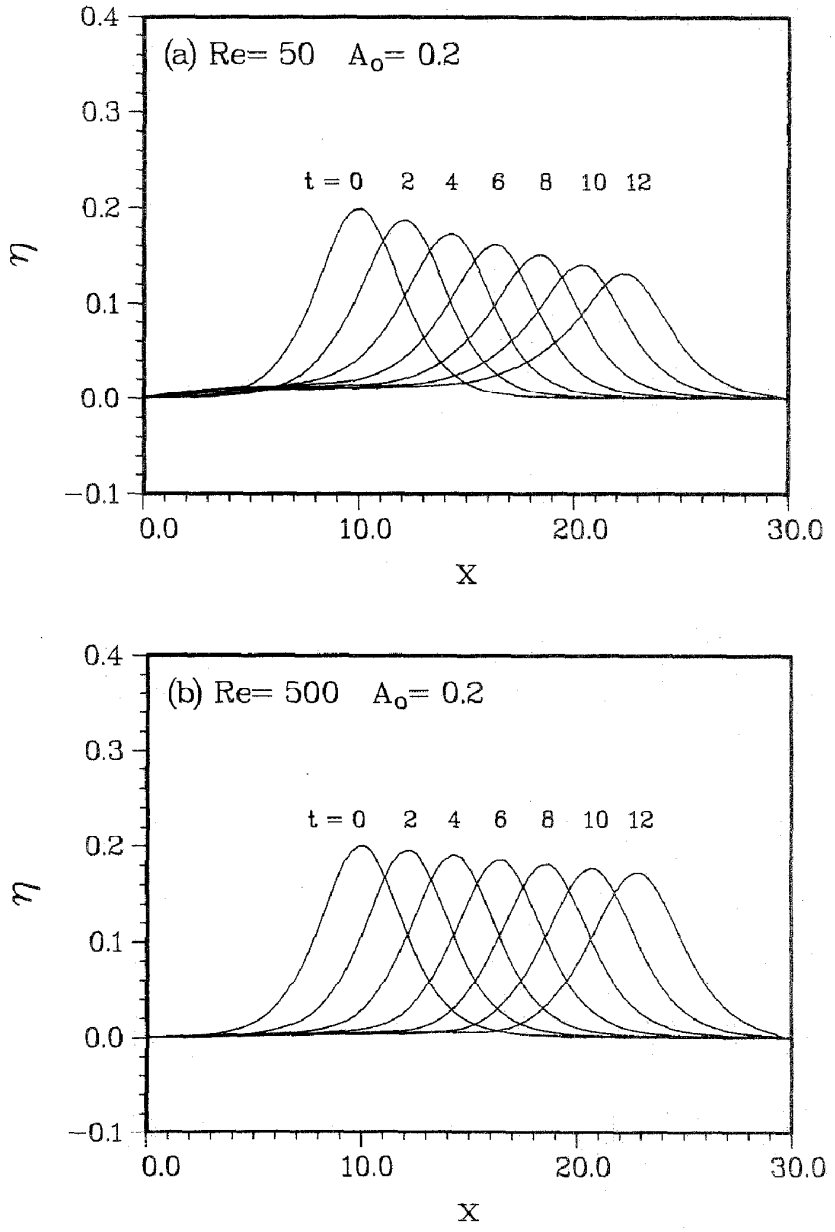

FIG. 4. Evolution of wave profiles at different Reynolds numbers.

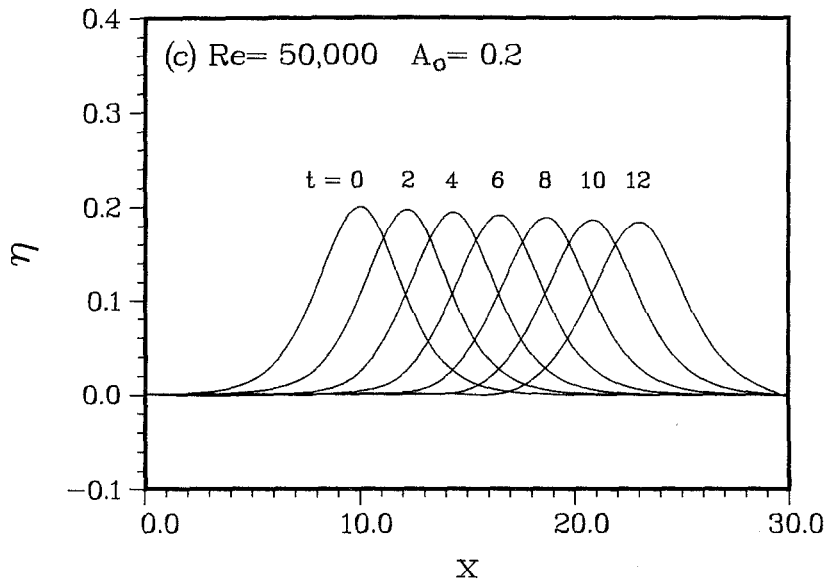

FIG. 4. (*Continued*)

where A_0 and A are the initial and damped wave lengths, respectively, t is the travel time of the wave, and Re is the Reynolds number based on the velocity $\sqrt{gh}$ and water depth h in the channel. This expression is claimed to be compatible with Russell's experimental data for a solitary wave in water and will be compared with the numerical solutions.

In the present calculations, viscous damping by both the bottom and the free surface are considered because the full Navier–Stokes equations are solved with the nonslip condition at the channel bottom and the complete kinematic and dynamic (including viscosity and surface tension) conditions at the free surface. A solitary wave, with initial free-surface profile given by Eq. (14) and $A_0 = 0.2$, was initialized at the position $x_0 = 10.0$ at $t = 0$ and then allowed to propagate in the positive direction of the x-axis. The calculation domain was taken to be the region between $x_u = 0.0$ and $x_d = 30.0$, with 62×30 grid points in the x and y directions, respectively, as shown in Fig. 3. The solution was marched up to $t = 12$ in 120 time steps, each with $\Delta t = 0.1$, and about five iterations at each time step were required to ensure that the free-surface elevation had converged to within 10^{-5} of the reference value h. Calculations performed with different time steps indicated little sensitivity of the final results for this wave amplitude.

The numerical results for the free-surface elevation between $t = 0$ and $t = 12$, at intervals of 2 time units, are shown in Fig. 4 for three values of the Reynolds number, Re = 50, 500, and 50,000. It is clear that the viscous damping of the wave decreases with increasing Reynolds number.

An essential result of linear theory of waves in a viscous fluid [7] is that the

viscous effect attenuates only the wave amplitude, without affecting the wave length, velocity, or phase [8]. However, this is not true for a nonlinear wave of finite amplitude, such as a solitary wave in a channel. The viscous effect causes the wave amplitude, wave length, velocity, and phase all to change of the wave travels in the channel. From Fig. 4 it is found that the wave crest lags by small but increasing amounts as the Reynolds number decreases. This is presumably due to the stronger nonlinearity of the free surface, and the relatively greater dissipation of energy at the bottom and the free surface at low Reynolds numbers. The latter will tend to reduce the wave amplitude and, consequently, the velocity of propagation of the wave.

The calculated attenuation of the wave crest with distance traveled by the wave is shown in Fig. 5. The numerical predictions with the grid shown in Fig. 3 are consistent with Eq. (39) and the limitations of the theory.

Typical distributions of velocity, pressure, vorticity and rate-of-strain for $\mathrm{Re} = 500$ at $t = 6$ are shown in Fig. 6a–d. The velocity field shown in Fig. 6a is similar to that calculated from potential theory in regions remote from the boundaries. The corresponding pressure distribution (Fig. 6b) is smooth but has a hump just below the wave crest. This hump moves with the wave.

Figure 6c shows where vorticity is generated and how it diffuses. There are two sources of vorticity, one at the channel bottom and the other at the free surface, the former being much stronger. At the free surface the vorticity is most intense at positions of maximum curvature. This is consistent with the results of Patel,

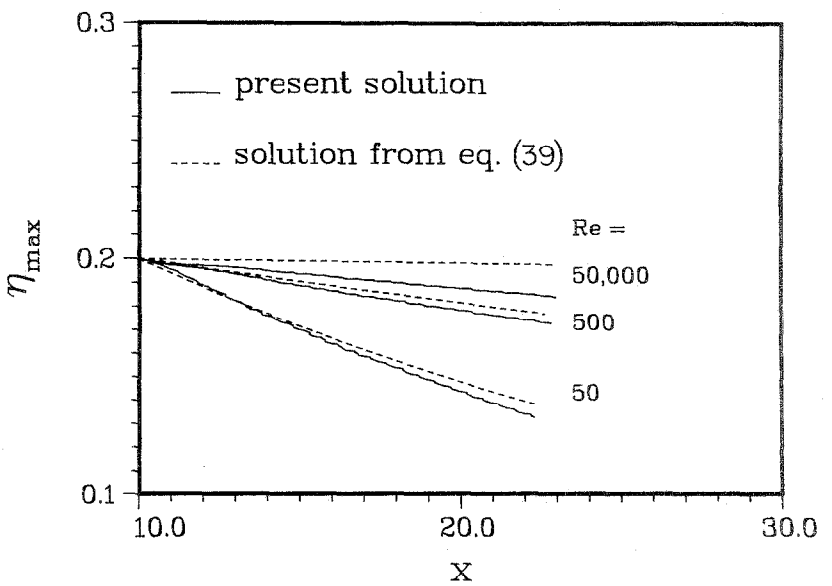

FIG. 5. Damping of wave height with distance.

Landweber, and Tang [9] obtained from the theory of the free-surface boundary layer. As the Reynolds number is increased (results not shown), the vorticity becomes more concentrated and is intensified. This is true for the vorticity generated in the boundary layer at the channel bottom as well as that at the free surface. At large times, the point of minimum vorticity at the bottom moves in phase with the wave peak while the vorticity which has diffused far from the bottom lags behind the wave crest. A region of vorticity of opposite sign (with positive

[redacted]

interest to examine the distribution of the rate of strain. This is shown in Fig. 6d. We see that the rate of strain is associated only with the nonslip condition at the bottom. In other words, the vorticity at the free surface has no rate of strain associated with it.

5. Reflection of the Wave at a Vertical Wall

The second problem we shall consider is that of reflection of the wave from a vertical wall. An incident solitary wave, of initial height A_0 at $x = x_0$ in a channel of unit depth, propagates in the x-direction towards a vertical wall located at $x = x_d$ and is reflected, as shown in Fig. 7. The numerical solutions will be compared with the inviscid solutions of Meneses and Chwang [10], who, in turn, have compared their results with the experimental observations of Chan and Street [11] and Maxworthy [12], and the results of linear theory.

The inviscid solution for this problem was obtained by Meneses and Chwang [10] by a perturbation method. The two small parameters for asymptotic expansions in their theory are: the ratio of the incident wave amplitude A_0^* to the water depth, i.e., $A_0 = A_0^*/h \ll 1$, and the ratio of the water depth to the wave length λ, i.e., $(h/\lambda) \ll 1$; but with the Ursell number, $Ut = A_0^* \lambda^2/h^3$, they are assumed to be of the order of unity. The solution for the surface profile can then be expressed as

$$\begin{aligned}\eta = A_0[&\operatorname{sech}^2(L+\delta_1) + \operatorname{sech}^2(R+\delta_2) \\ &+ A_0(\tfrac{1}{2}\operatorname{sech}^2 L \operatorname{sech}^2 R - \tfrac{3}{4}\operatorname{sech}^2 L \tanh^2 L \\ &- \tfrac{3}{4}\operatorname{sech}^2 R \tanh^2 R)],\end{aligned} \tag{40}$$

where

$$\begin{aligned} L &= \tfrac{1}{2}(x - x_0 - \beta)\sqrt{3A_0} \\ R &= \tfrac{1}{2}(x - 2x_d + x_0 + \beta)\sqrt{3A_0} \\ \delta_1 &= \tfrac{1}{4}A_0(\tanh R - 1) \\ \delta_2 &= \tfrac{1}{4}A_0(\tanh L + 1) \\ \beta &= (1 + A_0/2)\, t. \end{aligned}$$

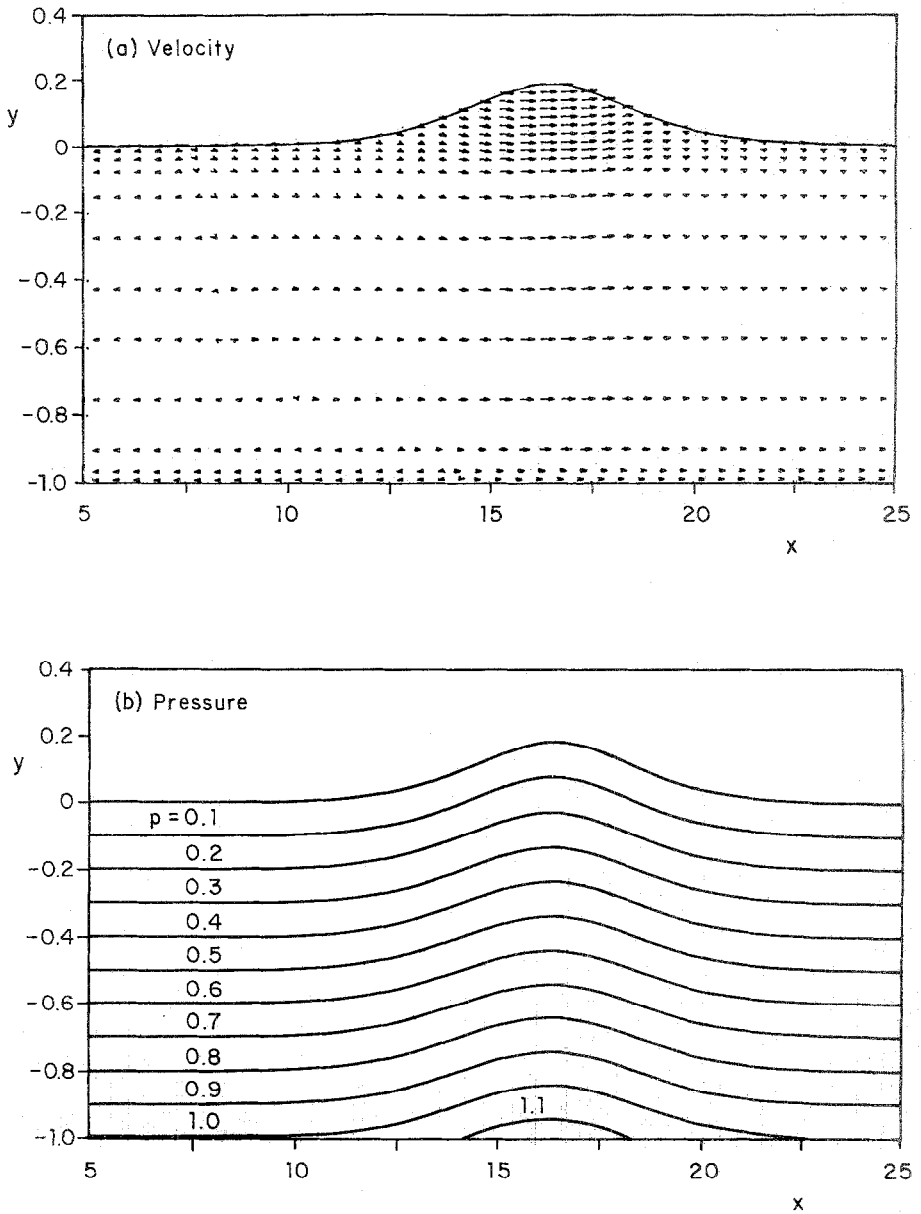

FIG. 6. Typical solution field at an instant of time.

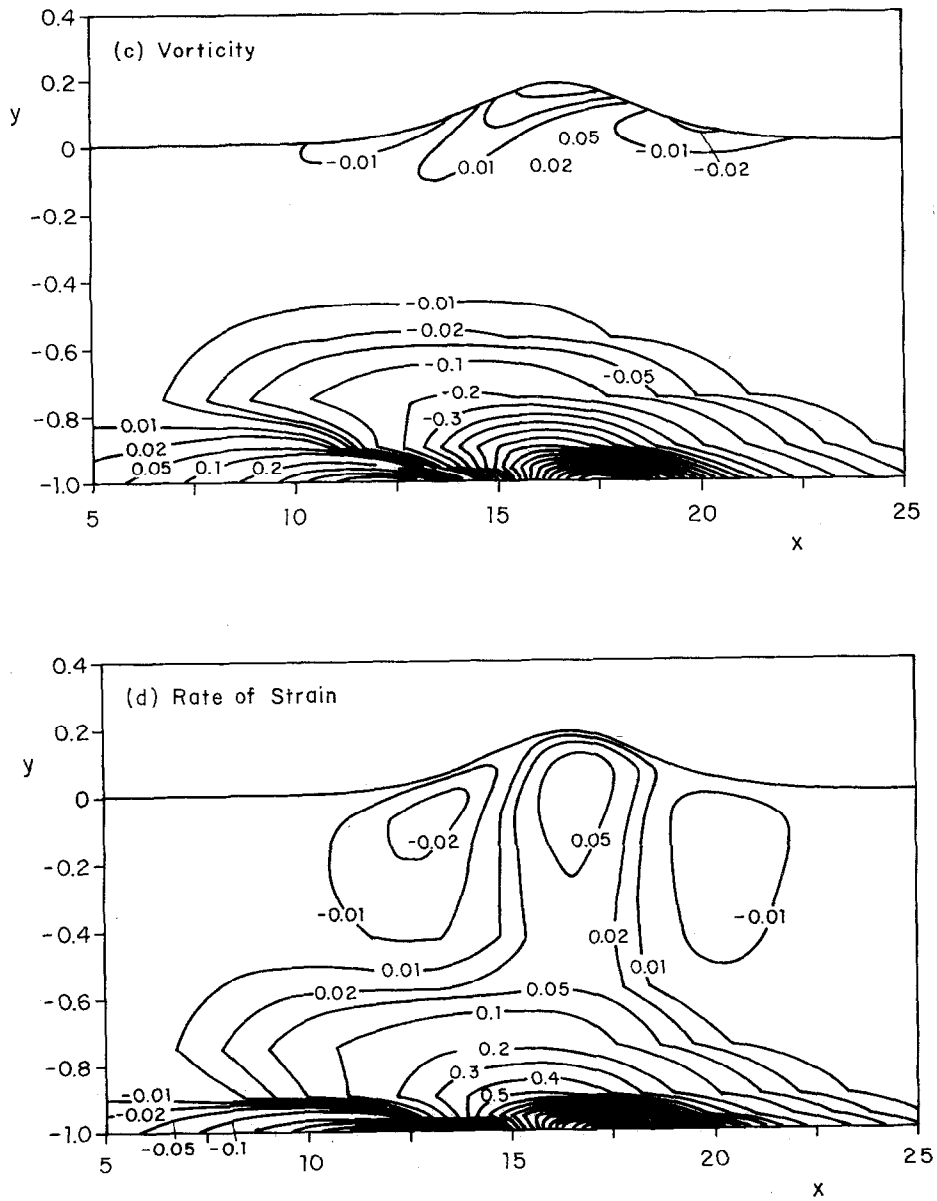

FIG. 6. (*Continued*)

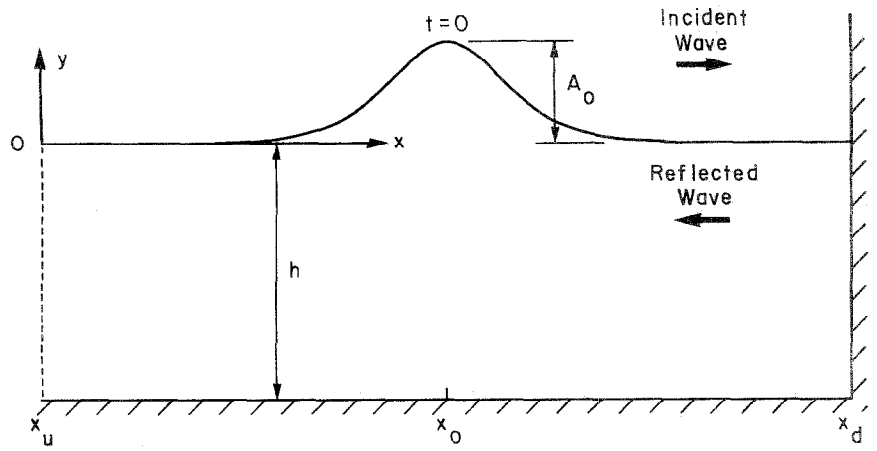

FIG. 7. Notation for wave reflection from a vertical wall.

The above parameters have been modified to apply to the present coordinate system. The maximum amplitude occurs at

$$t_{\max} = (x_1 - x_0 + \tfrac{1}{2}\sqrt{A_0/3})/(1 + \tfrac{1}{2}A_0). \tag{41}$$

The duration δt for which the crest of the wave remains at the wall is

$$\delta t = \frac{1.52}{\sqrt{A_0}}\,[1 + O(A_0)]$$

and the phase shift, δx, after reflection is

$$\delta x = \sqrt{A_0/3}\,[1 + O(A_0)].$$

These theoretical results of Meneses and Chwang [10] compared well with the experiments of Maxworthy [12] and Chan and Street [11].

For the numerical calculations, the initial free-surface profile and velocity field were specified in the same way as in the previous case. Waves with A_0 in the range 0.1 to 0.5 with the crest at $x_0 = 10$ at $t = 0$, were calculated. The vertical wall is at $x_d = 20$ and the solution domain extended from $x_u = 0$ to $x_d = 20$, as shown in Fig. 7. The Reynolds number based on channel depth and $\sqrt{gh}$ chosen for all calculations of this section is 50,000. The calculations were carried out over 160 time steps, with $\Delta t = 0.1$, and 5 iterations at each step. It should be remarked that,

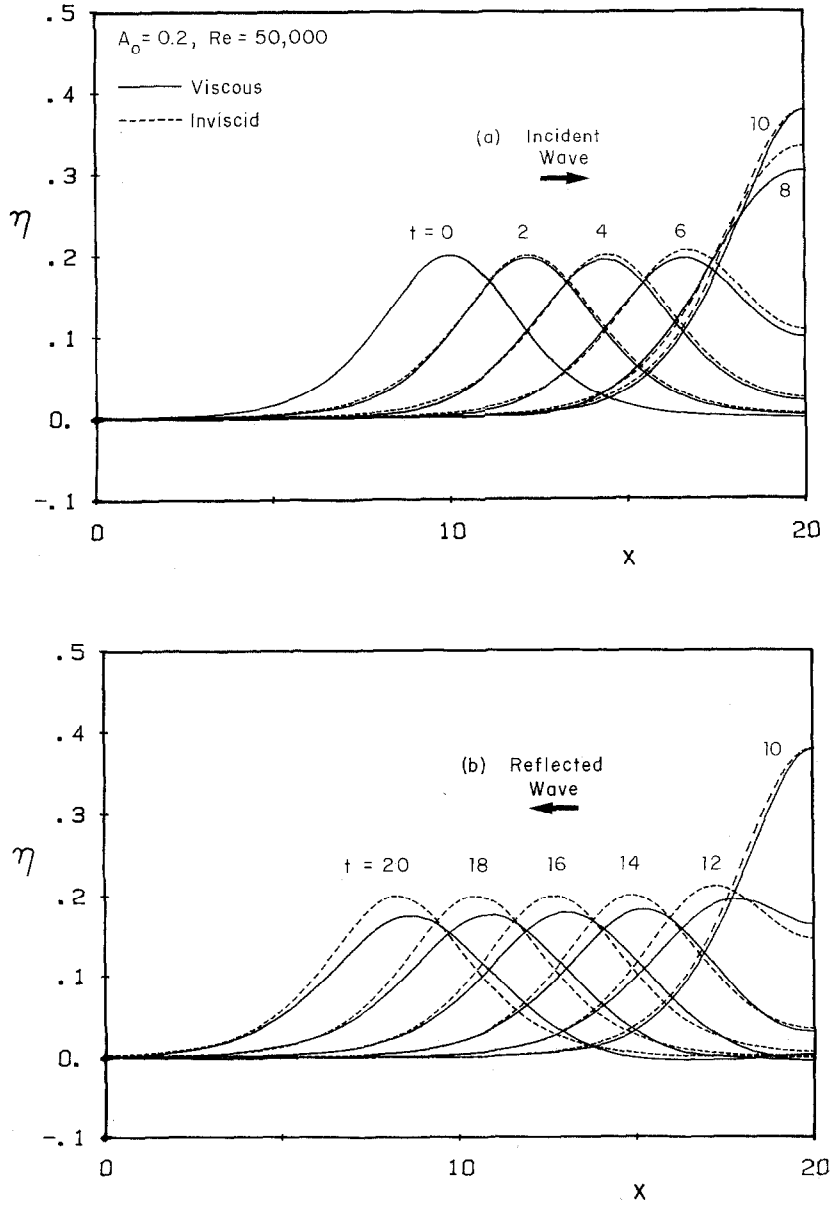

FIG. 8. Free-surface profiles during wave reflection.

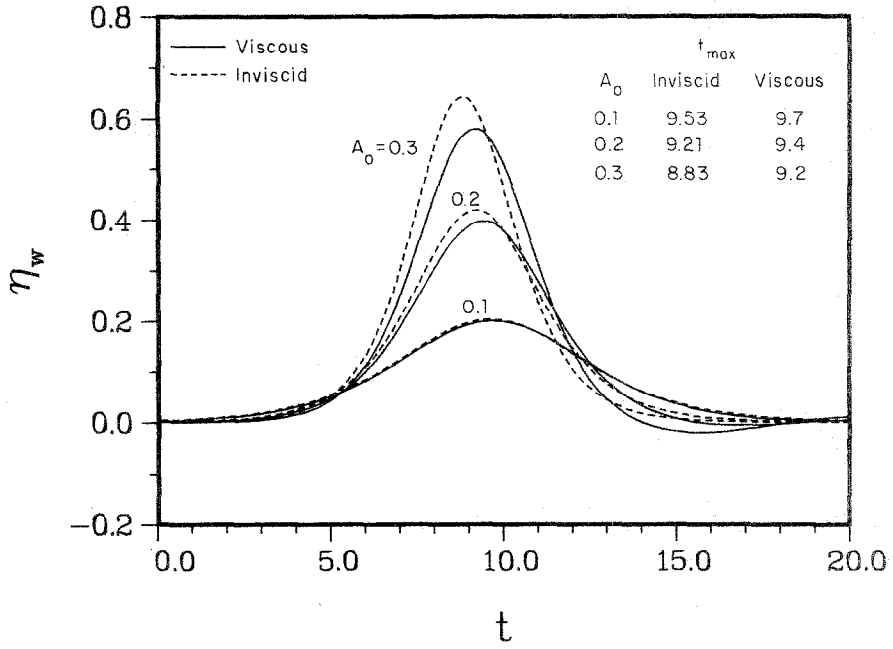

FIG. 9. Time variation of wave run-up at the wall.

as discussed in Section 1, the conditions $\partial v/\partial x = 0$ and $u = 0$ were used at two nodes just beneath the free surface to determine the contact point along the vertical wall.

The time evolution of the free-surface profile is shown in Fig. 8 for the case of $A_0 = 0.2$. The present viscous solution is compared with the inviscid result of Eq. (40). As expected, the influence of viscosity is to decrease the wave amplitude and speed in the course of the reflection. The run-up height at the wall is plotted against time in Fig. 9. The table in this figure shows the time t_{max} for the maximum run-up, from both the present numerical calculations (denoted as "viscous" in the table) and the inviscid-flow results (Eq. (41)). The occurrence of the maximum run-up for inviscid flow is slightly earlier than that for viscous flow. This is because the attenuation of the wave amplitude in viscous flow delays the propagation toward the wall. Figure 10 shows the relation between the incident-wave height and the maximum run-up at the wall. The present results are shown only up to $A_0 = 0.3$ because, for steeper waves, it was not possible to assure solution accuracy with the chosen grid. In this figure, comparisons of the present numerical results with those obtained from experimental data, the inviscid-flow results of Meneses and Chwang and the linear solution are shown. It is found that the present method gives consistent and satisfactory results.

The time evolution of the velocity field during reflection for the case of $A_0 = 0.2$

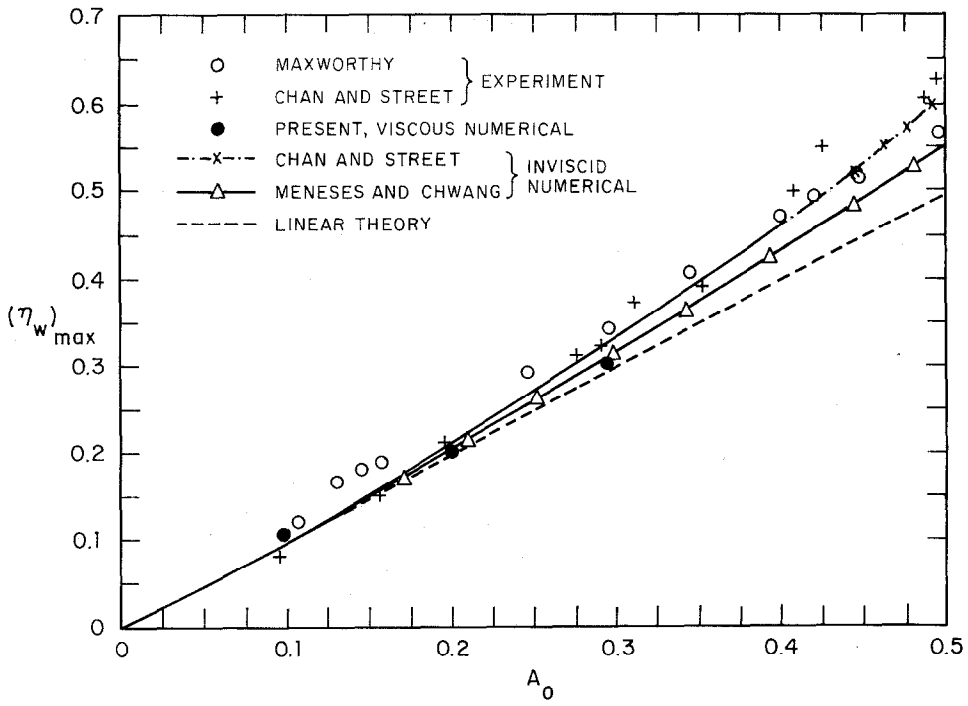

FIG. 10. Maximum run-up versus incident wave amplitude.

toward the wall with the vertical velocity increased, then becomes stationary, and, finally, descends and accelerates in the reflected direction. The effect of the wall at a point is approximately equivalent to the superposition of two identical waves, of wave length large compared with the water depth, approaching each other. This implies that the path of a fluid particle is approximately an ellipse about its mean position (see Lamb [7]). This property is consistent with the numerical results shown in Figs. 6a and 11.

Finally, it is of interest to note that all calculations reported here were carried out on a Prime 9955 computer. A typical calculation, with a 62×30 grid and 150 time steps, required between 30 and 40 min of cpu time.

6. CONCLUSIONS

We have presented a numerical method for the solution of the unsteady, two-dimensional, Navier–Stokes equations for flows involving a free-surface. Two problems, concerned with solitary waves, have been treated and the results compared with available experimental data and other theoretical solutions. These show

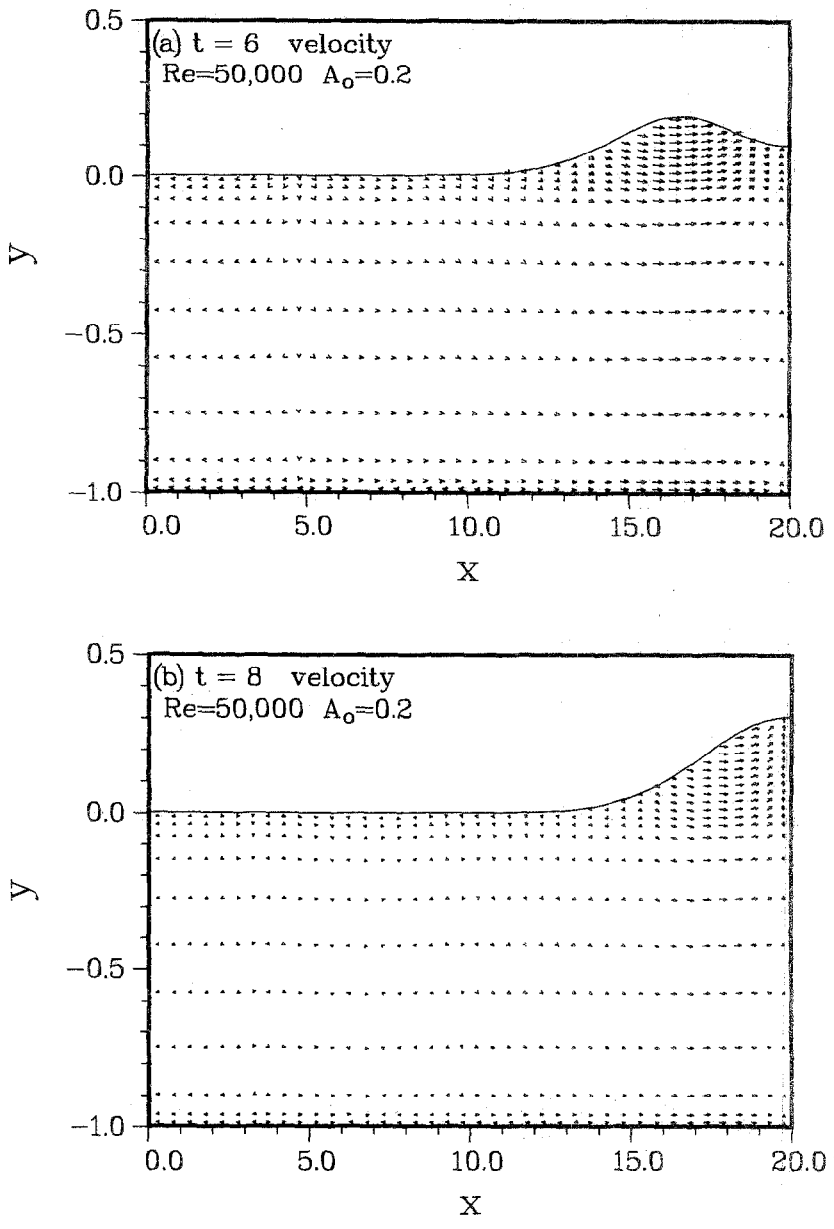

FIG. 11. Velocity field during wave reflection.

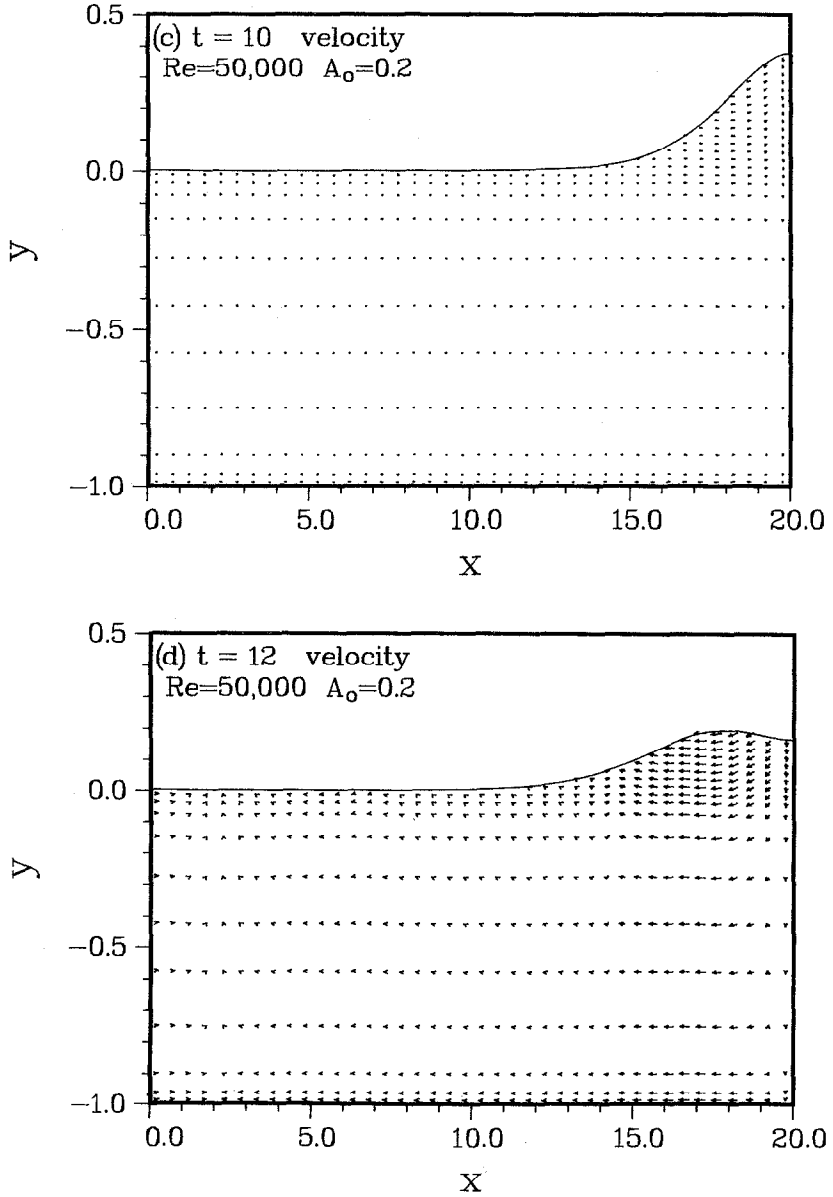

FIG. 11. (*Continued*)

that the present approach yields satisfactory results. With regard to the numerical method, we note that greater accuracy can be achieved by replacing the simple five-point finite-analytic formulation used for the momentum equations with the more complete nine-point formula. Also, boundary-fitted coordinates, moving with the free surface, could be used to further increase the accuracy, especially for waves with large curvature and slope.

ACKNOWLEDGMENTS

This research was sponsored by the Office of Naval Research, Accelerated Research Initiative (Special Focus) Program in Ship Hydrodynamics, under Contract N00014-83-K-0136. The authors are grateful to Dr. H. C. Chen for many helpful discussions on numerical methods.

REFERENCES

1. F. H. HARLOW AND J. E. WELCH, *Phys. Fluids* **8**, 2182 (1965).
2. R. K. CHAN AND R. L. STREET, Technical Report No. 135, Dept. of Civil Eng., Stanford Univ., 1970 (unpublished).
3. S. V. PATANKAR, Numerical Heat Transfer and Fluid Flow (McGraw-Hill, New York, 1980), p. 131.
4. C. J. CHEN AND H. C. CHEN, *J. Comput. Phys.* **53**, 210 (1984).
5. G. H. KEULEGAN, *J. Res. Nat. Bur. Standards* **40**, (1948).
6. C. C. MEI, The Applied Dynamics of Ocean Surface Waves (Wiley, New York, 1983), p. 564.
7. H. LAMB, *Hydrodynamics* (Dover, New York, 1932), p. 364.
8. C. R. DEPRIMA AND T. Y. WU, Report No. 21-23, California Inst. Technology, Pasadena, CA, 1957 (unpublished).
9. V. C. PATEL, L. LANDWEBER, AND C. J. TANG, in Proceedings Second International Symposium on Ship Viscous Resistance, Goteborg, Sweden, 1985 (SSPA, Marine Research and Consulting, 1985), p. 23.
10. H. P. MENESES AND A. T. CHWANG, Report No. 251, Iowa Inst. of Hydraulic Res., University of Iowa, Iowa City, IA, 1982 (unpublished).
11. R. K. CHAN AND R. L. STREET, *J. Comput. Phys.* **6**, 68 (1970).
12. T. MAXWORTHY, *J. Fluid Mech.* **76**, 177 (1976).